PAPER

Preparation and flash memory performance based on fluorene–triphenylamine copolymer (PF–TPA)/MWCNTs†

Qun Yang,[a] Xiankai Jiang,[a] Ying Xin,[a] Xiaofeng Zhao,[c] Jiahe Huang,[a] Shuhong Wang, [ID] *[a] Rongrong Zheng,[b] Dongge Ma[d] and Cheng Wang [ID] *[ab]

A conjugated alternating polymer based on fluorene and triphenylamine, namely poly[(9,9-dioctyl)-2,7-fluorene-*co*-triphenylamine] (PF–TPA), in which triphenylamine (TPA) as electron donor and hole transporting group was devised and synthesized on the basis of the Suzuki coupling method. The structural properties of the copolymer can be verified by Fourier transform infrared (FT-IR) spectroscopy, hydrogen and carbon nuclear magnetic resonance (^{1}H-NMR, ^{13}C-NMR). Nonvolatile memory devices with bistable electrical switching behavior were observed based on active layers of both fluorene–triphenylamine copolymer (PF–TPA) and PF–TPA:carbon nanotubes (CNTs) hybrid composite materials. Typical formed composite-based device with sandwich configuration, indium tin oxide (ITO)/PF–TPA:CNTs/Al, was demonstrated superior rewritable flash memory property compare to the ITO/PF–TPA/Al device with a greater ON/OFF state current ratio. In addition, the optimal storage characteristics occurs when the doping concentration of CNTs was at a certain value (CNTs = 0.3 mg mL^{-1}), which leading to the ON/OFF state current ratio added up to 2 orders of magnitude and the switching threshold voltage reduced prominently. The conductance switching mechanism of devices was also further discussed. After testing, the devices have good stability and durability, which have a potential application value in data storage.

1. Introduction

Resistive random access memory (RRAM) based on organic films with resistive switching effects has attracted intense attention from scholars in the recent two decades.[1] Owing to the advantages of easy processing, high storage density, low cost, low power consumption, and high mechanical flexibility,[2–5] organic storage, which is different from traditional semiconductor silicon based electrical memory,[6] has become an emerging electrical memory technology and has developed rapidly.[7] Generally speaking, the organic resistive memories realize the transition of different conducting states by applying an external voltage to both ends of the organic functional layer film, and the OFF state and ON state are equivalent to the "0" and "1" in binary systems.[8] Moreover, nanocomposite

[a]Key Laboratory of Functional Inorganic Material Chemistry, Heilongjiang University, Harbin 150080, P. R. China. E-mail: wangc_93@163.com; openair@163.com

[b]School of Chemical Engineering and Materials, Heilongjiang University, Harbin 150080, P. R. China

[c]School of Electronic Engineering, Heilongjiang University, Harbin 150080, P. R. China

[d]School of Materials Science and Engineering, South China University of Technology, Guangzhou 510640, P. R. China

† Electronic supplementary information (ESI) available. See DOI: 10.1039/c7ra11905d

materials, because of their attractive properties, were considered as a promising candidate for the next generation of nonvolatile memory devices, and the addition of inorganic nanomaterials further optimizes the electrical and optical properties of the matrix, promoting organic polymer/inorganic nanocomposite materials with broad commercial development and application prospects.[9–11]

In recent years, polymers and their composites with carbon nanotubes have been gradually applied to the field of organic electronics memory which due to the unique hybrid structure and attractive physical properties of carbon nanotubes.[12–14] Large numbers of RRAM based on polymers have been developed by adding carbon nanotubes, including poly(*N*-vinylcarbazole) (PVK),[15] polyvinyl alcohol (PVA),[16] poly-4-vinylphenol (PVP),[17] poly(3,4-ethylenedioxythiophene):poly(styrenesulfonate) PEDOT:PSS,[18,19] epoxy methacrylate resin (EMAR),[20] polyurethane (PU).[21] These researches made different attempts to mix carbon nanotubes into organic films and reasonable conjecture that the amount of carbon nanotubes doped cause some memories exhibited distinctly different resistance behaviors. For example, G. Liu *et al.* found that the device produces insulator behavior (0.2% CNTs), bistable electrical switching behavior (0.5–2% CNTs), and conductor behavior (≥3% CNTs)[15] by manipulating the content of carbon nanotubes in the PVK layers; then Pandurangan *et al.* once

again confirmed the three similar electrical behaviors of PVA film joined with 0.1% CNTs, 1–3% CNTs and ≥5% CNTs, respectively.[16] In addition, a current bistability was shown in the PEDOT:PSS matrix with a small quantity of functionalized multiwalled carbon nanotubes (MWCNTs) (≤0.01 wt%).[18] Subsequently, researchers continued to investigate the effects of different levels of SWCNTs on the bi-directionally memory behavior in the identical matrix,[19] nonvolatile memory characteristics in EMAR + CNTs and PU + CNTs composite film have gradually been developed.[20,21] Although much work has been reported on the effects of electrical switching and memory effects in doped or mixed polymer with inorganic nanoparticles systems, the influence of dope level on the conductance behavior of polymeric composites seems to be worth further exploration.[22,23]

As the hole-transporting materials, polyfluorene (PF) and its derivatives have become one of the most promising candidates for organic memory devices (OMDs).[24] The fluorene group, as a good luminescent material, has higher carrier mobility and carrier transport along its conjugated backbone.[25,26] The triphenylamine (TPA) group in the main chain was used as electron donor, which helped to enhance the hole transport ability and thermal stability of the polymer, was a typical hole transporting material.[27] Therefore, copolymer containing fluorene or triphenylamine groups have attracted considerable attention as electrical storage materials.[28,29] In this study, we first synthesized the conjugated alternating copolymer poly[(9,9-dioctyl)-2,7-fluorene-co-N-4,4′-triphenylamine] (i.e., PF–TPA) by Suzuki coupling reaction and characterized the copolymer by various tests. Then the nonvolatile bistable conductor switching behavior and rewritable flash memory effects in both ITO/PF–TPA/Al and ITO/PF–TPA:CNTs/Al memory devices were discovered. The performance of the nonvolatile memory, which fabricated by the PF–TPA + CNTs with different doping levels as an active layer, improved to a certain extent compared with the ITO/PF–TPA/Al device. It can be obviously perceived that the electrical memory characteristics was significantly improved with the higher ON/OFF current ratio (increased from 10^2 to 10^4) and lower threshold voltage (V_{SET} reduced from -2.4 V to -1 V) in a specific concentration (CNTs = 0.3 mg mL^{-1}) by adding CNTs into PF–TPA matrix. No significant attenuation occurs in current during the retention and endurance tests illustrated that the presence of CNTs enables the device to remain stable. Finally, the electrical characteristics were analyzed by reasonable simulation and our fabricated devices exhibits preeminent flash and reliability characteristics.

## 2. Experimental

2.1 Materials

All of the organic solvents and reagents were purchased from Sinopharm Co. Ltd. The sodium carbonate was dehydrated and the toluene was distilled over sodium under dry nitrogen. MWCNTs were disposed by acidification treatment. The outer diameter of the tube was 17–23 nm and the length of the tubes was several μm. The micro-structure analysis of CNTs was exposed by means of transmission electron microscopy (TEM) research, as shown in Fig. S1.† All other chemicals were provided by Sigma-Aldrich without further purified.

2.2 Synthesis of poly[(9,9-dioctyl)-2,7-fluorene-co-triphenylamine] (PF–TPA)

Scheme 1 shows the synthetic route and the chemistry structure of PF–TPA. 9,9′-Dioctyfluorene-2,7-diboronic acid bis(1,3-propanediol)ester (0.5000 g, 0.8954 mol), 4,4′-dibromo-triphenylamine (0.3608 g, 0.8954 mmol) and toluene (14 mL) were added into a flask which was by removal of water and deoxidization in advance. After the reaction mixture was dissolved, tetrakis(triphenylphosphine)palladium(0) [Pd(PPh$_3$)$_4$] (0.0310 g, 2.686 × 10^{-2} mmol) as catalyst and sodium carbonate solution (3 mol L^{-1}, 14 mL) were added into the flask rapidly, accompanied with the gradual heating from 95 °C to 105 °C and kept stirring and refluxing under nitrogen atmosphere for 48 h. The organic layer was washed several times with deionized water and concentrated by rotatory evaporator after the solution cooled, then dropped the obtained product into methyl alcohol to precipitate the desired product. The product was accumulated by negative-pressure filtration and washed with methyl alcohol. Finally the copolymer was extracted by acetone in soxhlet extractor for 48 h to remove the remaining monomers and Pd catalyst and dried in a vacuum dying oven. The dried

Table 1 Different dosages of mixture as composite film

Sample	CNTs (mg)	PF–TPA (mg)	Isopropyl alcohol (mL)	Toluene (mL)
A	0	5	0	1
B	0.1	5	1	1
C	0.3	5	1	1
D	0.5	5	1	1
E	1.0	5	1	1
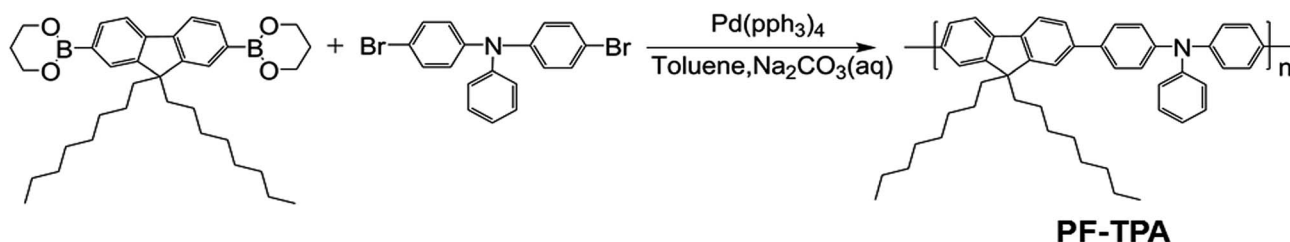
Scheme 1 Synthesis routes and the chemistry structure of copolymer (PF–TPA).
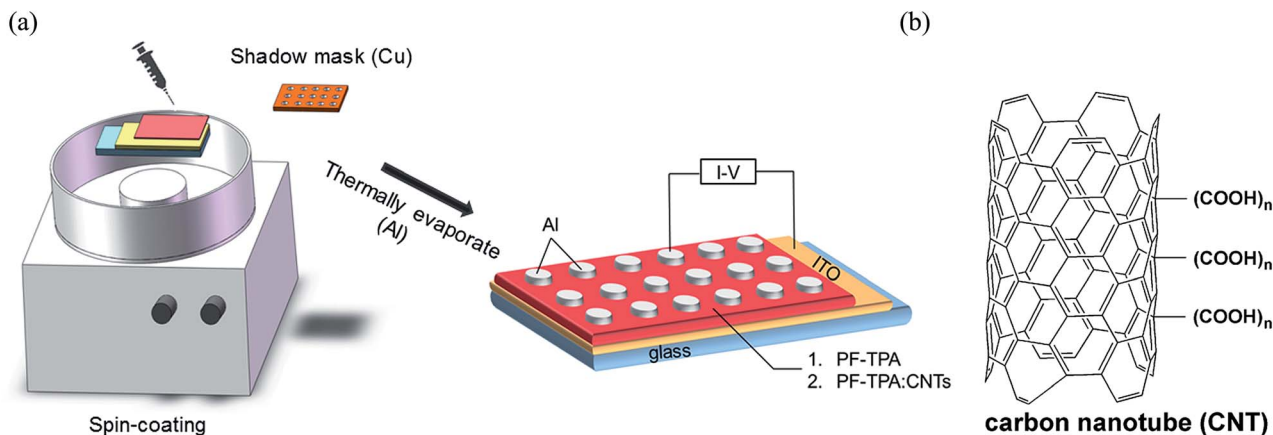
Fig. 1 (a) Schematic diagram of the sandwich-structured device. (b) Chemistry structure of carbon nanotube (CNT).

product was characterized by FT-IR spectroscopy, ^{1}H-NMR and ^{13}C-NMR analyzes.

2.3 Fabrication of the memory device

Before spin-coating the film, the indium tin oxide (ITO) conductive glass of dimension 2 cm × 1 cm (sheet resistance $R \leq 10\ \Omega\ \square^{-1}$) were preprocessed gradually with deionized water, abstergent, acetone and ethanol for 30 min each by ultrasonication and stored in a vacuum drying oven at 60 °C for 12 h. The PF–TPA ($M_w = 26\ 000$) with different carbon nanotubes doping content is used as the active layer of the device. Synthetic copolymer PF–TPA was dissolved in toluene with stirring and filtered through a 0.22 μm pore size of polytetrafluoroethylene membrane syringe filter to prepare a homogeneous solution.

For manufacture the blended composites, MWCNTs was disperse in isopropanol and keep ultrasonication for 50 min. Afterwards, the same volume of MWCNTs dispersion and the pretreatment of PF–TPA solution were mixed together and persistently stirred for 1 h. Different dosages of mixture as composite film samples were shown in Table 1, which were spin-coated onto the ITO conductive glass substrate at a rotate speed of 900 rpm for 15 s and then 3000 rpm for 45 s.

After that, the semi-finished films were dried in a vacuum oven at 60 °C for 2 h to get rid of remaining solvent. The film thickness of pure PF–TPA and PF–TPA:CNTs composite were revealed by scanning electron microscope (Hitachi S3400) measurement before vacuum aluminizing. Al electrode was used in vacuum thermally evaporation under a shadow mask at 7.5 × 10^{-7} Torr with diameter of 200 μm. The elementary diagram of sandwich-structured device and the chemistry structure of MWCNTs were displayed in Fig. 1.

2.4 Measurements

The FT-IR spectra were indicated on Magna-IR560 infrared spectrometers with KBr pellet from 400–4000 cm^{-1} wavenumbers. ^{1}H NMR and ^{13}C NMR spectra were measured on a Bruker Advance 400 NMR spectrometer with deuterated chloroform as the solvents of 400 MHz resonance frequency.

The molecular orbitals were calculated by the density function theory (DFT) using Parr correlation functional method (B3LYP) and the 6-31G basis set. The electrical memory characteristics of the device was disposed on an analytical probe station by a Keithley 4200-SCS semiconductor parameter analyzer at room temperature in the exposed atmospheric environment. Two probes were in contacted with the top electrode (Al) and the grounded bottom electrode (ITO) throughout the whole process of scanning voltage (applied voltage from 6 V to −6 V) with the step of 0.05 V. In the meantime, a current of 0.1 A was exerted in order to keep off the collapse of the device.

3. Results and discussion

3.1 Characterization of the copolymer PF–TPA

The dried copolymer PF–TPA was weighed to 0.4667 g and the yield of product is 82.54%. Furthermore, the product was characterized by FT-IR spectroscopy, ^{1}H-NMR and ^{13}C-NMR analyzes.

We analyzed the existence of bonds in PF–TPA by FT-IR spectroscopy, in which the instrument was a Magna-ir560 infrared spectrometer, and the results were shown in Fig. S2.† It is found that the characteristic absorption peak in 2922 cm^{-1} and 2850 cm^{-1} are due to the C–H stretching vibration of the fluorene in PF–TPA. In addition, the absorption peaks at 1511 cm^{-1} and 1464 cm^{-1} wavenumbers are ascribed to the C=C skeleton vibrations of PF–TPA. Moreover, the existence of absorption peaks at 1273 cm^{-1} is attributed to the C–N stretching vibration in triphenylamine.

The ^{1}H-NMR of PF–TPA was shown in Fig. S3.† ^{1}H-NMR (400 MHz, CDCl$_3$) δ_H (ppm): 7.75 (d, $J = 7.8$ Hz, 2H), 7.62–7.55 (m, 8H), 7.31 (t, $J = 7.7$ Hz, 2H), 7.25–7.21 (m, 6H), 7.07 (t, $J = 7.4$ Hz, 1H), 2.08–1.99 (m, 4H), 1.29–0.98 (m, 24H), 0.79 (t, $J = 7.0$ Hz, 6H).

The ^{13}C-NMR of PF–TPA was shown in Fig. S4.† ^{13}C-NMR (100 MHz, CDCl$_3$) δ_H (ppm): 151.67, 147.57, 146.89, 139.81, 139.35, 135.92, 129.37, 127.86, 127.19, 125.56, 124.53, 124.27, 120.95, 119.94, 55.25, 40.49, 31.79, 30.91, 30.06, 29.22, 23.85, 22.60, 14.06.
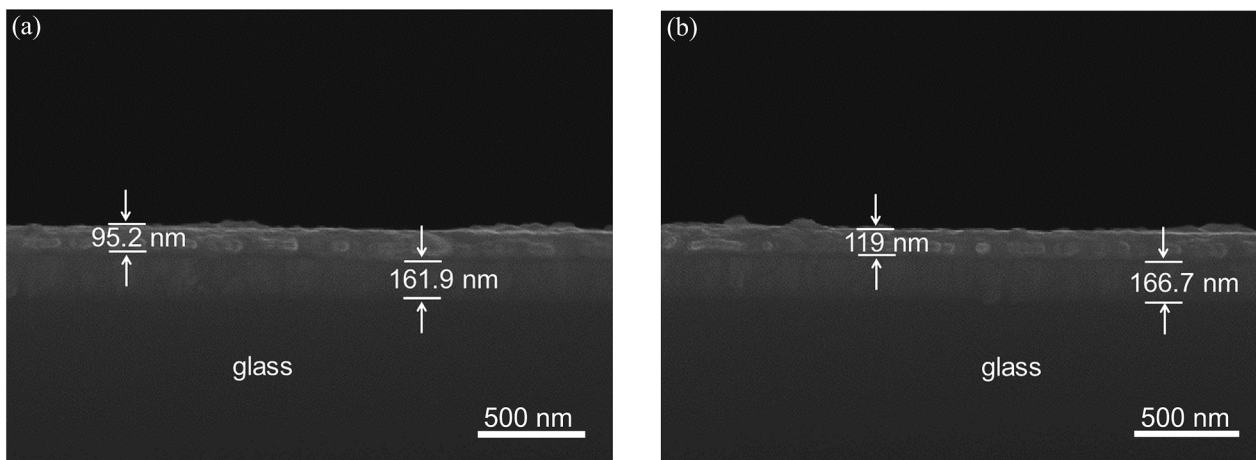
Fig. 2 Cross-section scanning electron microscopic images of the device based on (a) PF−TPA and (b) PF−TPA/MWCNTs composite films.

Furthermore, the copolymer (M_w = 26 000) was characterized by gel permeation chromatography (GPC) using a Malvern instrument which attached to a single refractive index detector (Vis-cotek-VE3580-RI Detector). The THF solution with a flow rate of 1 mL min^{-1} at 35 °C was used as the mobile phase and the standard samples of polystyrene was used for calibration, that the number-average molecular weight (M_n), weight-average molecular weight (M_w), polydispersity (PDI) and the average degree of polymerization (n) of PF–TPA was identified as 15 000, 26 000, 1.73 and 23.8, respectively.
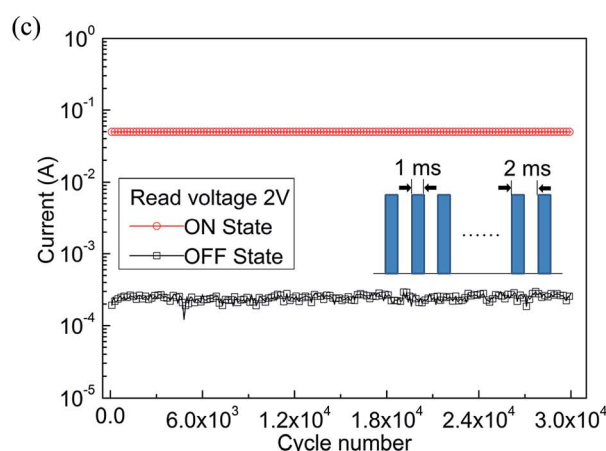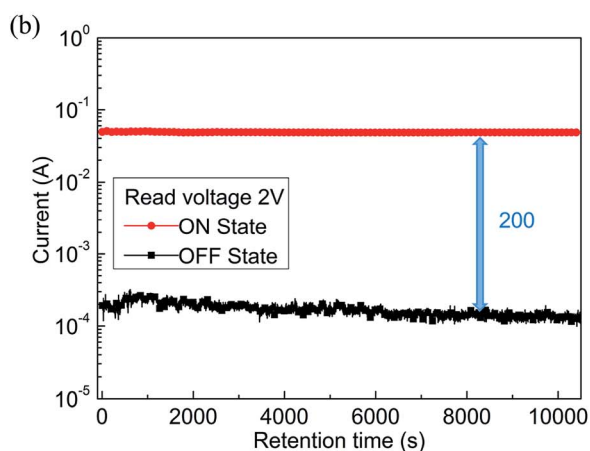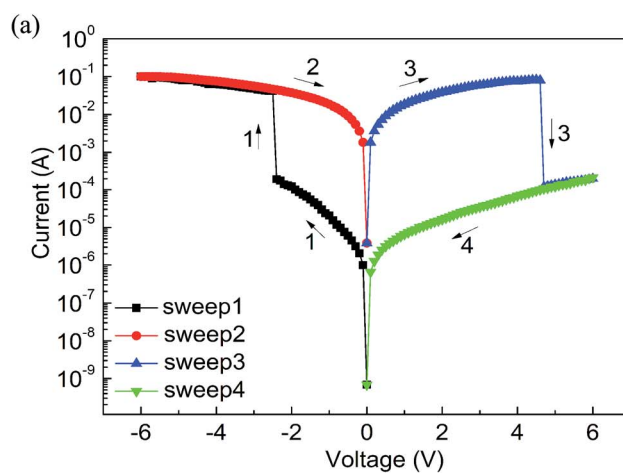

Fig. 3 (a) I−V curves, (b) retention performance and (c) endurance performance of ITO/PF−TPA/Al device.
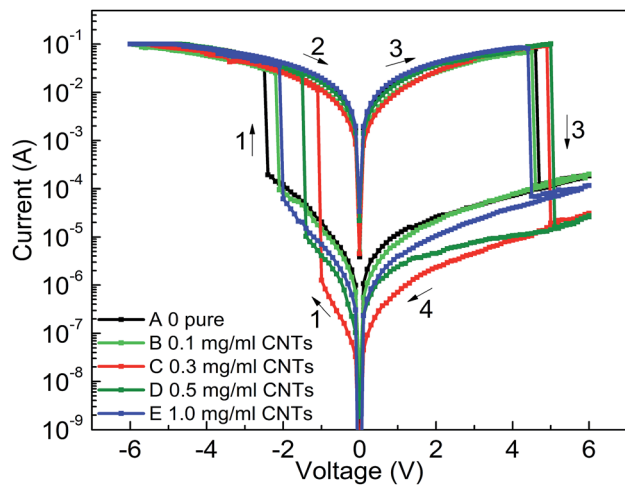
Fig. 4 *I–V* curves of ITO/PF–TPA:CNTs/Al with different CNTs doping level (0 mg mL^{-1}, 0.1 mg mL^{-1}, 0.3 mg mL^{-1}, 0.5 mg mL^{-1}, 1.0 mg mL^{-1}).

3.2 Cross-section characteristics of two types of devices

The film thickness of both composites were revealed by means of scanning electron microscope (SEM) research, as shown in Fig. 2. The sandwich structure of the device can be observed with homogeneous film and well-arranged layers. The thickness of active films of PF–TPA and PF–TPA:CNTs are measured as 95.2 nm and 119 nm, respectively.

3.3 Characterization of the ITO/PF–TPA/Al memory device

3.3.1 Current–voltage characteristics. The current–voltage characteristics curve detected electrical conductance behaviors and memory performance of these devices. For the sake of determining the impact of hybrid materials and their doping level, a separate investigation was applied to the ITO/PF–TPA/Al undoped device (sample A). As shown in Fig. 3a, four steps scan constituted a typical *I–V* characteristic curve with the different

applied voltage range varied from 0 to −6 V, −6 to 0 V, 0 to 6 V and 6 to 0 V. Initially, with the increase of the applied voltage during the first sweep, the current increased gently, suddenly a sharp current came up around −2.4 V, and the device was switched from high resistance state (HRS) to low resistance state (LRS). The conduction process at this time corresponds to the process of "writing" in the digital memory. In this moment, the device turned into the ON state with ON/OFF current ratio up to 2 × 10^2 and then the LRS state remained in the subsequent second rescan (sweep 2), which progress according with "reading" step. Subsequently a reverse bias from 0 to 6 V in the third sweep, when the applied positive bias reached a certain value, the current in high conductive state (ON state) went abruptly downward and backed to the primitive low conductive state (OFF state) near 4.6 V impressed voltage. The corresponding progress from LRS to HRS is defined as "erasing". The fourth sweep followed the third scan bias, the curve demonstrated a uniform trend of low conductive state and extend outwardly ("rereading" progress). Two segment processes of current which dramatically increased and decreased in the above, were also called "SET" and "RESET", respectively. Furthermore, the rewritable electrical characteristics generated by four-step sweep constituted the entire write–read–erase–reread" (WRER) circulation process, both the SET and RESET showed nonvolatile characteristics, indicating a flash-type memory.

3.3.2 Retention and endurance performances. In order to verify the retention and endurance properties of the device, the following tests and results are shown in Fig. 3b and c. When the constant voltage of 2 V was applied, the current was always maintained in the vicinity of the initial value and no significant attenuation was observed over 3 h in both LRS and HRS, the ON/OFF current ratio retains about 2 × 10^2 at 2 V. Moreover, the current kept stable for up to 3 × 10^4 continuous cycle numbers under the read pulses of 2 V (pulse period = 2 ms, pulse width = 1 ms). These results represented the device with favorable stability and reliability.
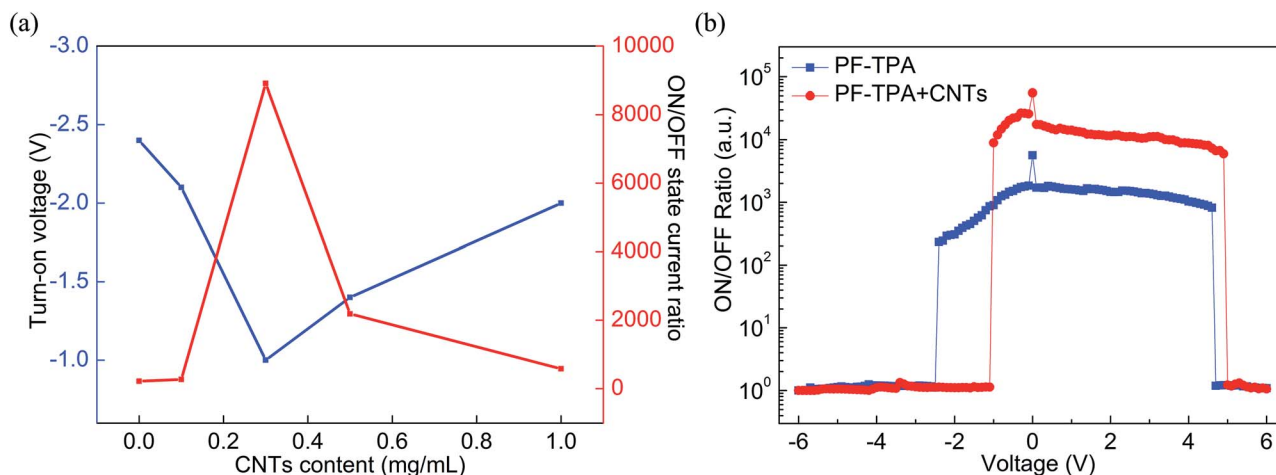

Fig. 5 (a) The ON/OFF current ratio and threshold voltage of ITO/PF–TPA:CNTs/Al devices with different CNTs concentration. (b) The ON/OFF current ratio of ITO/PF–TPA:CNTs/Al devices and the ITO/PF–TPA/Al device.
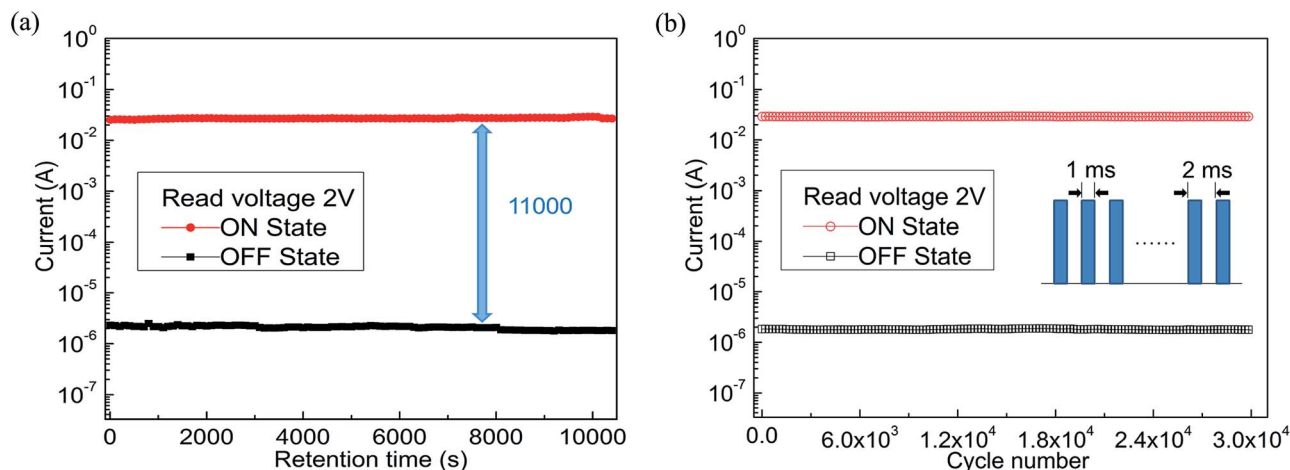
(a)

(b)

Fig. 6 (a) Retention performance and (b) endurance performance of ITO/PF–TPA:CNTs/Al device on sample C.

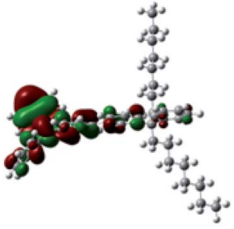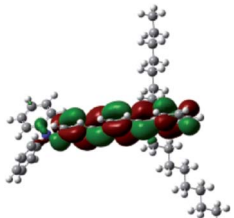## 3.4 Characterization of the ITO/PF–TPA:CNTs/Al memory device

3.4.1 Current–voltage characteristics. According to the measurement result of pure organic materials device hereinabove, we attempted to select diversified concentration of CNTs solution repeatedly (Table 1). All the prepared organic–inorganic nanocomposite devices manifested the similar conductive properties. As shown in Fig. 4, an external negative bias was applied from 0 to -6 V via the top electrode induced a current uprush near -2.1 V and the negative bias earned the device always in ON state. Since then, a conversely tendency was exhibited in the next positive bias application process. During the whole cyclic process, the ON/OFF current ratio sustained about 2.7×10^2 (sample B). The electrical memory characteristic curve based on sample C disclosed a homologous flash phenomenon. A noticeable current changing abruptly made the device transform between LRS and HRS, the threshold voltage was around -1 V and -4.8 V, and the ON/OFF current ratio reached a stable level of 10^4. For sample D, a precipitate jumping and dropping current was occurred around -1.4 V and 4.9 V, achieved a switching ratio of 2×10^3. As the same characteristics (sample E), when the extrinsic voltage scanned in -2 V and 4.4 V for the singular sweep, an abrupt current lifting through the circulation with the ON/OFF current ratio of 6×10^2.

Combined with these comparative experiments, we draw the following conclusions. Fig. 5a records the influence of doping concentration both threshold voltage and switching ratio by the double Y curve. The composite device with CNTs shows different levels of electrical memory performance in both threshold voltage and ON/OFF current ratio. Therefore, the incorporation of CNTs was a critical factor to reduce the threshold voltage and increase the switching ratio. Significantly, with the increase of doping level, the ON/OFF current ratio increased and then decreased after reaching a maximum. This may be due to the specific conductivity of CNTs to be well dispersed in film surface to form electron transport pathways. With increasing doping concentration, the effective distance of the isolated CNTs decreases. When the effective distance is less

than the diameter of individual carbon nanotube, a homogeneous two-phase interface is favorable for formation to produce more electron transport pathways. When the threshold voltage is approaching, a large number of electrons passing through the increased number of carrier pathways, which cause a switching current ratio increasing phenomenon.[15]

However, we analyze that the excessive concentration dopant will lead to the formation of minimum distances between isolated nanotubes, which affects the charge carrier transport along the electron path and becomes not easy to jump through the nanotube, bringing about a smaller current ratio.[15] Meanwhile, the threshold voltage continues to decrease until a minimum value appears at the same concentration. This is because the smaller distance of carbon nanotubes can make effective carrier hopping with lower activation energy.[15] Fig. 5b shows the most marked growth in flash window at a given concentration (0.3 mg mL^{-1}) in contrast with the Al/PF–TPA/ITO device as a comparative study.

Table 2 Molecular simulation result for PF–TPA

Frontier molecular orbital	Energy level (eV)
HOMO	-5.00
LUMO	-1.27

3.4.2 Retention and endurance performances. Furthermore, we tested the retention and endurance performances of the device with the optimal storage effect. As shown in Fig. 6a, with an initial voltage sweep of 2 V in atmospheres, two states currents based on sample C can be levelled off over 3 h and the ON/OFF current ratio maintains approximately 1.1×10^4, indicating that the composite material has outstanding stability. Besides, as shown in Fig. 6b, the current exhibited no degradation more than 3×10^4 cycle numbers in 2 V pulse, suggesting that the read cycles have no influence on HRS and LRS states. All of the above test reveals a fact that the performance of ITO/PF–TPA:CNTs/Al memory device compares favorably with single-layer polymeric memory device. With the addition of CNTs, the threshold voltage of ITO/PF–TPA:CNTs/Al reduced from −2.4 V to −1 V and the ON/OFF current ratio shows an enhancement of 2 orders of magnitude in comparison with the ITO/PF–TPA/Al memory device.

3.5 Molecular simulation and electronic transition mechanism

3.5.1 Quantum chemical calculation. Some physical properties of polymers, such as molecular orbitals, energy levels, can be conveniently obtained by computation.[30] In order to further explore the electronic structure of polymers and corresponding charge transfer process, we calculate HOMO, LUMO and the energy band gap ($\Delta E = E_{\text{LUMO}} - E_{\text{HOMO}}$) of PF–TPA by DFT (B3LYP/6-31G) calculations. E_{HOMO} is related to molecular electron donating ability, and E_{LUMO} expressed the ability of molecules to accept electrons, which determine the way the molecule interacts.[31,32] Since the calculation of multiple derived in this paper was theoretically estimated.

The electronic ground state of the copolymer was optimized by DFT, and we can see the theoretical energy level data and the simulation results in the Table 2. The HOMO electron cloud is mainly distributed in the triphenylamine moiety and extended to conjugate chains, suggesting that the TPA unit has a strong electron donating capability for hole migration. And the LUMO electron cloud is concentrated in the conjugated chain of fluorene. The HOMO, LUMO, and the band gap of PF–TPA was calculated to the energy value of −5.00, −1.27 and 3.73 eV by B3LYP/6-31G model chemistry, respectively.

3.5.2 Mechanism of ITO/PF–TPA/Al and ITO/PF–TPA:CNTs/Al memory device. In order to further explore the electrical conductance switching behavior and the mechanism of two types of memory devices, we redrew the *I–V* characteristic
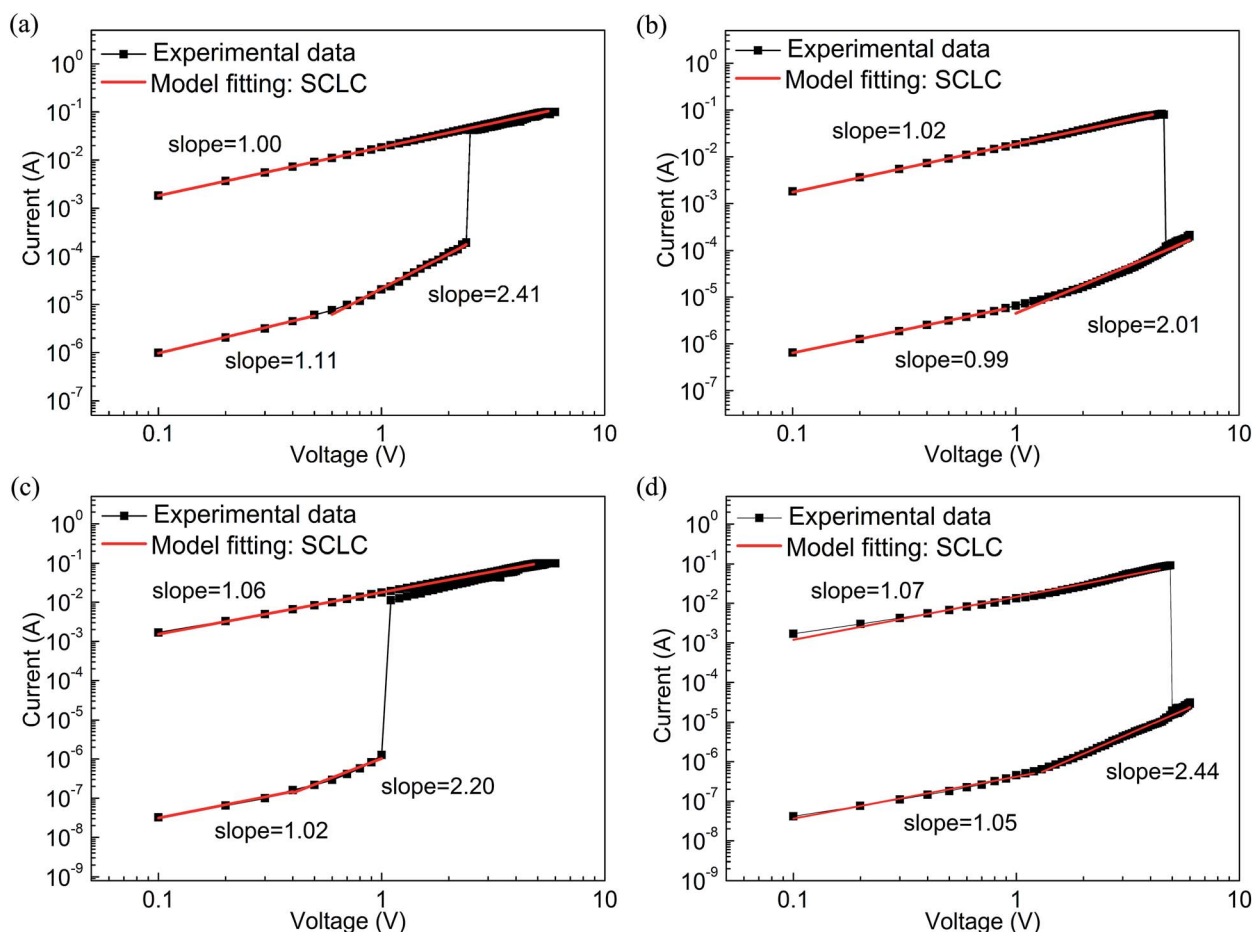

Fig. 7 Linear fitting and corresponding slopes for Al/PF−TPA/ITO (a) set, (b) reset and for Al/PF−TPA:CNTs/ITO device based on sample C. (c) Set, (d) reset.

curve with log–log plotting and performed the corresponding curve fitting. Fig. 7 shows the slope of the fitted curve on high resistance state (HRS) and low resistance state (LRS), which include both Al/PF–TPA/ITO and Al/PF–TPA:CNTs/ITO nonvolatile memory devices. As shown in Fig. 8a and b, for Al/PF–TPA/ITO device, fitting curves of two segments traced along the straight in ON state with the slope of 1.00 (set) and 1.02 (reset), respectively. This indicates that the transmission mechanism could be follows Ohm's law (slope approximate to 1) with a linear relationship of $I \propto V$. In the OFF state, the slope of double logarithmic curve is close to 1 at low applied voltage (slope = 1.11 for set segment and 0.99 for reset segment), then a steeper slope forms in the second high voltage region (with the slope of 2.41 and 2.01), in other words, the current is proportional to the square of the voltage ($I \propto V^2$), indicating that the conduction behavior in this region changed into the Child's law. Based on the above data analysis, we can conclude that the switching behaviour of Al/PF–TPA/ITO may be dominated by the trap-limited space-charge limited current (SCLC).[33]

At the other side of Al/PF–TPA:CNTs/ITO, the same conclusion can be inferred from the drawing results in Fig. 7c and d. The appearance of the slope (1.06 and 1.07) gives a phenomenon that the current varies linearly with the applied voltage in the ON state. It means that the relationship abide by the Ohm's law. For OFF state, similar ohmic conduction behavior was also observed under the low voltage location (slop = 1.02 for set and 1.05 for reset) and then transforms into the Child's law with the slope of 2.20 and 2.44 at the high applied voltage. We can also infer that the conductance mechanism is followed the trap-limited space-charge limited current (SCLC) in the Al/PF–TPA:CNTs/ITO device.[34,35]

3.5.3 Stored procedure of the ITO/PF–TPA/Al and ITO/PF–TPA:CNTs/Al memory devices. The energy level diagram of the Al/PF–TPA/ITO device and the possible carriers migration processes through the whole states was shown in Fig. 8a. When the negative voltage sweep occurs, ITO acts as an anode (−4.8 eV),[36] Al electrode is used as cathode (−4.27 eV).[36] The energy barrier between Al electrode and the LUMO level of the PF–TPA is 3.0 eV, which is much higher than the lowest energy barrier between the work function of ITO and the HOMO level of PF–TPA (0.2 eV), suggesting that hole injection from metal electrode into HOMO of the PF–TPA is a favorable process and the conduction process is more likely to be dominated by hole injection. As the voltage increases, the hole is gradually injected from ITO into HOMO and hoping along the conjugated polymer chains. The initial current exhibits slow growth under low voltage, which is due to the energy barrier between Al electrode and LUMO has a tendency of blocking electron migration. As the scan voltage increases, when the threshold voltage is reached, the electrons gain enough energy to overcome the energy barrier between Al electrode and LUMO to inject into the active film, that is to say, the electrons excite from HOMO to LUMO orbit, resulting an instant increase in the current. The charge passes through the filament and maintains its state. When reverse voltage is applied, a large amount of charge passes through the previously formed filaments. When the bias exceeds a certain value, the injected charge will exceed the

capacity of the filament and generate additional heat. Excessive currents result in repulsive coulombic interactions between the trapped charge in the organic active layer and the interface. The resulting heat and this repulsive coulombic interaction cause the filament to rupture and make the device make the device revert back to the OFF state.[37]

In view of the limited charge conduction capacity of polymers, carbon nanotubes are more likely as electron trapping center, introduced into the polymer active films to enhance charge injection and trapping.[25,36] As shown in Fig. 8b, in principle, the surfaced-modified CNTs has a work function of −5.1 eV (ref. 38) which is much lower than the LUMO energy level of PF–TPA, it means Al electrode contacts with carbon nanotubes to form an ohmic contact.[25] The electron injection from Al electrode into CNT is rather better than hole injection from ITO into the HOMO energy level of PF–TPA. Electrons are first injected from the Al electrode into the CNTs and transmitted along the CNTs axis. Under a certain scan bias, hole injection occurs, the carriers injected into the composite film and is captured by CNTs, resulting in the formation of a space charge layer. When the bias voltage reaches the threshold voltage, the carriers are injected into the polymer LUMO level along the nanotube axis through the film interface, causing
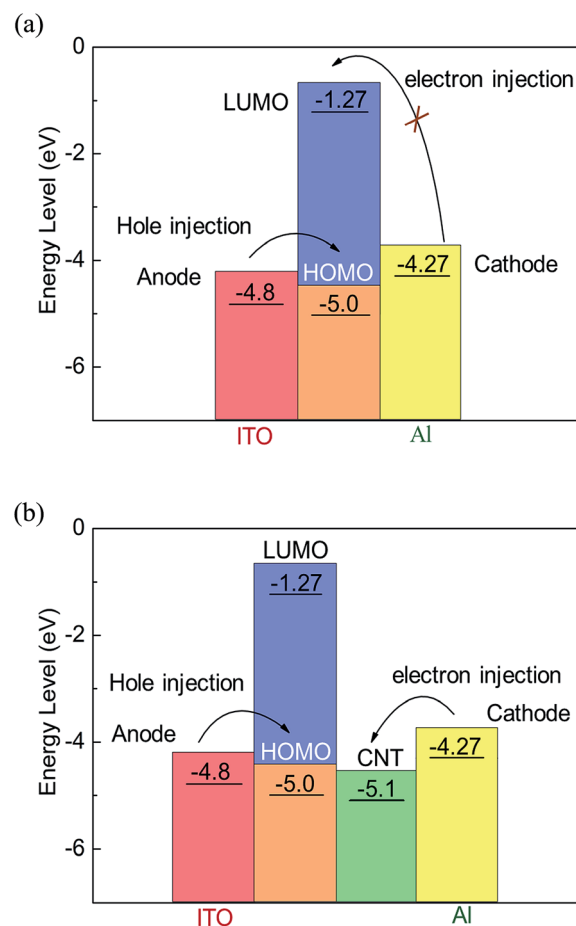

Fig. 8 Energy level diagram of the (a) Al/PF–TPA/ITO and (b) Al/PF–TPA:CNTs/ITO sandwich device.

a sudden increase in current. The content of CNTs in the device influences the effective distance of the neighboring CNTs, and then urge the trapping behavior of the charge carriers, which makes the devices exhibit different conductive behavior. Correspondingly, the additional heat produced by excessive charge conduction will cause the rupture of the conduction channel formed during the negative bias process, an nonvolatile bistable memory is obtained.

4. Conclusions

To conclude, we have effectively prepared the conjugated copolymers (PF–TPA) by Suzuki coupling reaction and applied to nonvolatile bistable memory device. The ITO/PF–TPA/Al memory device demonstrates excellent electrical storage properties and stability. The ON/OFF current ratio reaches 2×10^2 at low threshold voltage (-2.4 V). In addition, we also fabricated the nonvolatile memory devices utilizing PF–TPA:CNTs composite materials by a spin coating technique and explored the effects of different CNTs concentrations on devices, getting different bistable resistive flash devices. ITO/PF–TPA:CNTs/Al achieves preeminent electrical memory characteristics for that it improves the switching ratio (increased by two orders of magnitude) and reduces the threshold voltage (V_{SET} reduced from -2.4 V to -1 V) with lower error-tolerant rate. Meanwhile, the current remains stable over 3 h in 2 V applied voltage, as well as stable for up to 3×10^4 continuous cycle numbers in 2 V read pulse. The lower threshold voltage, higher switching ratio and excellent stability make the PF–TPA:CNTs composite material have potential application, and occupy the dominant position in the new generation of electrical memory devices.

Conflicts of interest

There are no conflicts of interest to declare.

Acknowledgements

Notes and references

1 Q. Liu, W. H. Guan, S. B. Long, R. Jia and M. Liu, *Appl. Phys. Lett.*, 2008, **92**, 012117.

2 U. S. Bhansali, M. A. Khan, D. Cha, M. N. AlMadhoun, R. Li, L. Chen, A. Amassian, I. N. Odeh and H. N. Alshareef, *ACS Nano*, 2013, **7**, 10518.

3 J. Y. Ouyang, C. W. Chu, C. R. Szmanda, L. P. Ma and Y. Yang, *Nat. Mater.*, 2004, **3**, 918.

4 T. Kurosawa, T. Higashihara and M. Ueda, *Polym. Chem.*, 2013, **4**, 16.

5 B. H. Lee, H. Bae, H. Seong, D. I. Lee, H. Park, Y. J. Choi, S. G. Im, S. O. Kim and Y. K. Choi, *ACS Nano*, 2015, **9**, 7306.

6 M. Kanoun, A. Souifi, T. Baron and F. Mazen, *Appl. Phys. Lett.*, 2004, **84**, 5079.

7 E. J. Yoo, M. Q. Lyu, J. H. Yun, C. J. Kang, Y. J. Choi and L. Z. Wang, *Adv. Mater.*, 2015, **27**, 6303.

8 G. Khurana, P. Misra and R. S. Katiyar, *J. Appl. Phys.*, 2013, **114**, 1625.

9 H. Ju and J. Kim, *Chem. Eng. J.*, 2016, **297**, 66.

10 B. Zhang, Y. Chen, G. Liu, L. Q. Xu, J. Chen, C. X. Zhu, K. G. Neoh and E. T. Kang, *J. Polym. Sci., Part A: Polym. Chem.*, 2011, **50**, 378.

11 X. Q. Guo, Y. K. Wang and R. Zhang, *Adv. Mater. Res.*, 2013, **634–638**, 1943.

12 R. H. Baughman, A. A. Zakhidov and W. A. de Heer, *Science*, 2002, **297**, 787.

13 W. J. Yu, A. H. Chae, S. Y. Lee, D. L. Duong and Y. H. Lee, *Adv. Mater.*, 2011, **23**, 1889.

14 J. P. Hollingsworth and P. R. Bandaru, *Appl. Phys. Lett.*, 2005, **87**, 814.

15 G. Liu, Q. D. Ling, E. Y. H. Teo, C. X. Zhu, D. S. H. Chan, K. G. Neoh and E. T. Kang, *ACS Nano*, 2009, **3**, 1929.

16 S. Chandrakishore and A. Pandurangan, *RSC Adv.*, 2014, **4**, 9905.

17 W. T. Kim, J. H. Jung and T. W. Kim, *Appl. Phys. Lett.*, 2009, **95**, 81.

18 J. A. Ávila-Niño, W. S. Machado, A. O. Sustaita, E. Segura-Cardenas, M. Reyes-Reyes, R. López-Sandoval and I. A. Hümmelgen, *Org. Electron.*, 2012, **13**, 2582.

19 Y. M. Sun, L. Li, A. Z. Wen, X. D. Bai and G. Li, *Phys. Chem. Chem. Phys.*, 2015, **17**, 17150.

20 B. Cho, T. W. Kim, M. Hoe, G. Wng, S. Song and T. Lee, *Org. Electron.*, 2009, **10**, 473.

21 B. Zhang, Y. L. Liu, Y. Chen, K. G. Neoh, Y. X. Li, C. X. Zhu, E. S. Tok and E. T. Kang, *Chem*, 2011, **17**, 10304.

22 X. Wang, W. Xie and J. B. Xu, *Adv. Mater.*, 2014, **26**, 5496.

23 L. Q. Xu, B. Zhang, Y. Chen, K. G. Heoh, E. T. Kang and G. D. Fu, *Macromol. Rapid Commun.*, 2013, **34**, 234.

24 H. C. Wu, A. D. Yu, E. Y. Lee, C. L. Liu and W. C. Chen, *Chem. Commun.*, 2012, **48**, 9135.

25 G. Liu, Q. D. Ling, E. T. Kang, K. G. Neoh, D. J. Liaw, F. C. Chang, C. X. Zhu and D. S. H. Chan, *J. Appl. Phys.*, 2007, **102**, 787.

26 A. Charas, J. Morgado, J. M. G. Martinho, L. Alcácer, S. F. Lim, R. H. Friend and F. Cacialli, *Polymer*, 2003, **44**, 1843.

27 Y. Shang, Y. Q. Wen, S. L. Li, S. X. Du, X. B. He, L. Cai, Y. F. Li, L. M. Yang, H. J. Gao and Y. L. Song, *J. Am. Chem. Soc.*, 2007, **129**, 11674.

28 T. Kuorosawa, C. C. Chueh, C. L. Liu, T. Higashihara, M. Ueda and W. C. Chen, *Macromolecules*, 2010, **43**, 1236.

29 T. W. Kim, S. H. Oh, H. Choi, G. Wang, H. Hwang, D. Y. Kim and T. Lee, *Appl. Phys. Lett.*, 2008, **92**, 253308.

30 Q. D. Ling, S. L. Lim, Y. Song, C. X. Zhu, D. S. H. Chan, E. T. Kang and K. G. Neoh, *Langmuir*, 2007, **23**, 312.

31 A. A. Nazeer, N. K. Allam, A. S. Fouda and E. A. Ashour, *Mater. Chem. Phys.*, 2012, **136**, 1.

32 M. Akhtaruzzaman, H. N. M. E. Mahmud, A. Islam, A. E. Shafei, M. R. Karim, K. Sopian, L. Y. Han and Y. Yamamoto, *Mater. Chem. Phys.*, 2013, **142**, 82.

33 H. Baek, C. Lee, J. Park, Y. Kim, B. Koo, H. Shin, D. Y. Wang and J. Cho, *J. Mater. Chem.*, 2012, **22**, 4645.

34 W. Kwon, B. Ahn, D. M. Kim, Y. G. Ko, S. G. Hahm, Y. Kim, H. Kim and M. Ree, *J. Phys. Chem.*, 2011, **115**, 19355.

35 G. F. Tian, D. Z. Wu, L. Shi, S. L. Qi and Z. Wu, *RSC Adv.*, 2012, **2**, 9846.

36 Q. D. Ling, Y. Song, S. L. Lim, E. Y. H. Teo, Y. P. Tan, C. X. Zhu, D. S. H. Chan, D. L. Kwong, E. T. Kang and K. G. Neoh, *Angew. Chem.*, 2006, **45**, 2947.

37 D. C. Guo, Z. Y. Sun, S. H. Wang, X. D. Bai, L. D. Xu, Q. Yang, Y. Xin, R. R. Zheng, D. G. Ma, X. F. Zhao and C. Wang, *RSC Adv.*, 2017, **7**, 10323.

38 H. Ago, T. Kugler, F. Cacialli, W. R. Salaneck, M. S. P. Shaffer, A. H. Windle and R. H. Friend, *J. Phys. Chem. B*, 1999, **103**, 8116.